X-ray diffuse scattering from a nitrogen-implanted niobium film

Satish I. Rao, C. R. Houska, K. Grabowski, G. Ice, and C. J. Sparks

---

Articles you may be interested in

Standing-wave-grazing-incidence x-ray diffraction from polycrystalline multilayers
Appl. Phys. Lett. **94**, 101909 (2009); 10.1063/1.3095496

X-ray scattering from misfit dislocations in heteroepitaxial films: The case of Nb(110) on Al 2 O 3
Appl. Phys. Lett. **78**, 443 (2001); 10.1063/1.1342215

Quasiparticle diffusion, edge losses, and back-tunneling in superconducting tunnel junctions under x-ray irradiation
J. Appl. Phys. **86**, 4580 (1999); 10.1063/1.371406

X-ray diffraction analysis of concentration and residual stress gradients in nitrogen-implanted niobium and molybdenum
J. Appl. Phys. **69**, 8111 (1991); 10.1063/1.347461

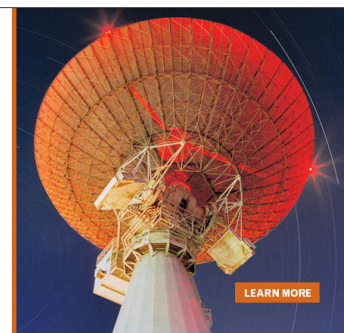Anomalous diffusion of nitrogen in nitrogen-implanted silicon
Appl. Phys. Lett. **54**, 1793 (1989); 10.1063/1.101266

X-ray diffuse scattering from a nitrogen-implanted niobium film

Satish I. Rao and C. R. Houska
Department of Materials Engineering, Virginia Polytechnic Institute and State University, Blacksburg, Virginia 24061

K. Grabowski
Naval Research Laboratory, Washington, DC 20375

G. Ice and C. J. Sparks
Oak Ridge National Laboratory, Oak Ridge, Tennessee 37831-6117

A 2500-Å niobium single-crystal film was deposited onto a sapphire substrate and subsequently implanted with nitrogen to an average concentration of 0.5 at. %. Synchrotron radiation was used to measure the difference between the implanted and an unimplanted film to isolate the diffuse scattering from the implanted film near two Bragg reflections. This diffuse intensity arises mainly from elastic displacement fields about radiation-damage-related loops located on (211) planes. A small contribution of the scattering is calculated from the displacements about single interstitial nitrogen in octahedral sites. The Burgers vector of the loops is along the [11$\bar{1}$] direction and makes an angle of 62° with the loop plane giving a dominant shear component. Vacancy loops have a radius ~5 Å while interstitials are somewhat larger ranging from 10 to 15 Å. The number of vacancies and interstitials are nearly the same.

I. INTRODUCTION

The structure of ion-implanted zones at high concentrations is complex and not well known. X-ray diffraction offers the possibility of examining zones nondestructively under the same stress conditions as the original implanted samples. Internal sources of stress can arise from the stress field of the implants themselves, as well as from knock-on defects produced by the energetic ions. To understand these two sources, further information is required about the atomic configurations of the stress-producing defects.

Under equilibrium conditions, N atoms become located at three equivalent octahedral positions in Nb.[1,2] This produces a major expansion of two first-neighbor lattice atoms along the *c* direction, and a smaller contraction of four second-neighbor lattice atoms.[2] This sizeable core disturbance produces lattice displacements like the highly anisotropic displacement field about a carbon atom in a bcc Fe lattice. Locating the *c* axis along three mutually perpendicular directions, maintains the overall cubic symmetry of the lattice.

Electron microscopy of thinned (stress relieved) samples shows the presence of small vacancy and self-interstitial loops ranging from 5 to 15 Å (Refs. 3 and 4) after neutron irradiation of Nb and Mo. It has been shown that for Ni-implanted Cu at liquid-He temperature, (LHT) these sources of internal stress almost cancel except for a stress contribution from the core region, i.e., near the circumference of the loop.[5,6] Both N interstitials and loops produce local displacements that decrease the integrated intensity of the Bragg peaks. This decrease may be associated with the appearance of diffuse scattering which is the primary focus of this paper.

X-ray intensity band analysis of N, implanted at liquid-nitrogen temperature (LNT) to an average of 5 at 0%,

revealed the presence of high biaxial compressive stresses along the implanted zone.[7,8] Evidence for some pointlike defects and defect clusters was obtained from attenuation factors determined by the displacement fields. X-ray diffuse scattering is known to be well suited for quantitative studies of pointlike defects and loop defects.[5,6,9–11] The displacement field from a loop is obtained from calculations by Ohr.[12] In this paper, x-ray diffuse scattering was measured about the (330) and (222) from a 2500-Å Nb crystal film oriented with the (111) plane parallel to the free surface. The N implantation resulted in an average concentration of 0.5 at. % N and ~6 major displacements per atom (dpa). At this lower concentration, the line broadening from the nonuniform *d* spacing was small enough to enable diffuse scattering to be measured close to the Bragg peaks. This is very weak for a film and required synchrotron radiation with relatively long counting times. Scattering calculations were based upon the elastic field from vacancy and interstitial loops, as well as implanted N, located in octahedral sites distributed equally over the three equivalent sites. Brief discussions of these results have been published in conference proceedings.[8]

II. THEORY

The primary equations given here, describing x-ray diffuse scattering from dislocation loops in cubic crystals, may be found in Refs. 5 and 6. The intensity of diffuse scattering from randomly distributed defect clusters, in the single-defect approximation, is given by[9–11]

$$I_{\text{diff}}(\mathbf{H}) = N_D |r_e f|^2 |A(\mathbf{H})|^2, \tag{1}$$

where r_e is the classical electron radius, f is the atomic scattering factor of the host lattice, $\mathbf{H} = h_1\mathbf{b}_1 + h_2\mathbf{b}_2 + h_3\mathbf{b}_3$ is the x-ray scattering vector, N_D

is the total number of defect clusters, and $A(\mathbf{H})$ is the scattering amplitude of the defect cluster which for a dislocation loop can be written as[5,6]

$$A(\mathbf{H}) = \sum_D \exp(i2\pi\mathbf{H}\cdot\mathbf{R}^D) + \sum_n \exp(i2\pi\Delta\mathbf{H}\cdot\mathbf{R}^n)$$
$$\times [\exp(i2\pi\mathbf{H}\cdot\mathbf{u}^n) - 1]. \tag{2}$$

The first sum is over the atoms in the loop situated at positions $\mathbf{R}^D$ and the second sum ranges over the atoms in the host lattice situated at positions $\mathbf{R}^{n'} = \mathbf{R}^n + u^n$, where $\mathbf{u}^n$ is the displacement of the nth atom relative to the regular periodic lattice position $\mathbf{R}^n$, due to the loop, $\Delta\mathbf{H} = \mathbf{H} - \mathbf{H}^0$, where $\mathbf{H}^0$ is the reciprocal lattice vector, $hb_1 + kb_2 + lb_3$ and h, k, and l are the Miller indices of the Bragg reflection. The Huang term is separated from the second term in Eq. (2) in the usual way:

$$A(\mathbf{H}) = \sum_D \exp(i2\pi\mathbf{H}\cdot\mathbf{R}^D) + i2\pi\mathbf{H}\cdot\mathbf{u}(2\pi\Delta\mathbf{H})$$
$$+ \sum_n \exp(i2\pi\Delta\mathbf{H}\cdot\mathbf{R}^n)\cdot[\exp(i2\pi\mathbf{H}\cdot\mathbf{u}^n)$$
$$- 1 - i2\pi\Delta\mathbf{H}\cdot\mathbf{u}^n]..., \tag{3}$$

in which $\mathbf{u}(2\pi\Delta\mathbf{H})$ is the Fourier-transformed displacement field. The scattering amplitude of Eq. (3) can be written as five separate components:

$$A(\mathbf{H}) = A_1^S(\mathbf{H}) + A_2^A(\mathbf{H}) + A_2^S(\mathbf{H}) + A_3^A(\mathbf{H})$$
$$+ A_3^S(\mathbf{H}), \tag{4}$$

where

$$A_1^S(\mathbf{H}) = \frac{\pi R_0^2 b_n}{V_e} \frac{2J_1(2\pi\Delta H_p R_0)}{(2\pi\Delta H_p R_0)} Q, \tag{5a}$$

$$A_2^A(\mathbf{H}) = -\frac{4\pi^2 H_i^0 G_{in} P_{nm}\Delta H_m}{V_c} \frac{2J_1(2\pi\Delta H_p R_0)}{2\pi\Delta H_p R_0}, \tag{5b}$$

$$A_2^S(\mathbf{H}) = -\frac{4\pi^2 \Delta H_i G_{in} P_{nm}\Delta H_m}{V_c} \frac{2J_1(2\pi\Delta H_p R_0)}{2\pi\Delta H_p R_0}, \tag{5c}$$

$$A_3^S(\mathbf{H}) = \frac{1}{V_c} \int_\mathbf{R} \cos(2\pi\Delta\mathbf{H}\cdot\mathbf{R})[\cos(2\pi\mathbf{H}\cdot\mathbf{u}) - 1]d\mathbf{R}, \tag{5d}$$

and

$$A_3^S(\mathbf{H}) = -\frac{1}{V_c} \int_\mathbf{R} \sin(2\pi\Delta\mathbf{H}\cdot\mathbf{R})[\sin(2\pi\mathbf{H}\cdot\mathbf{u}) - 2\pi\mathbf{H}\cdot\mathbf{u}]d\mathbf{R}. \tag{5e}$$

In deriving Eqs. (4) and (5a–5e) from Eq. (3), the lattice sums were written as integrals.[6] Einstein's summation convention is implied in Eqs. (5b) and (5c).[13] In Eqs. (5), b_n is the Burgers vector component perpendicular to the loop plane. R_0 is the radius of the circular loop, V_c is the volume of a lattice atom. J_1 is the Bessel function of order 1, ΔH_p is the projection of $\Delta\mathbf{H}$ on to the loop plane, Q is the phase factor for direct scattering from the loop which is $+1$ for interstitial loops and -1 for vacancy loops, G_{in} is

the Fourier transform of the elastic Green's function written in the cubic coordinate system, i.e.[6]

$$G_{in}(2\pi\Delta\mathbf{H}) = \frac{1}{(2\pi|\Delta\mathbf{H}|)^2}\left(\frac{\delta_{in}}{C_{44} + C_{an}e_n^2}\right.$$
$$- \frac{e_i e_n}{(C_{44} + C_{an}e_i^2)(C_{44} + C_{an}e_n^2)}$$
$$\left.\times\frac{C_{44} + C_{12}}{\{1 + \Sigma_k[(C_{44} + C_{12})/(C_{44} + C_{an}e_k^2)]e_k^2\}}\right). \tag{6}$$

$e_i = \Delta H_i/|\Delta\mathbf{H}|$, the C's are the elastic constants, and $C_{an} = C_{11} - C_{12} - 2C_{44}$, δ_{in} is the Kronecker δ function. P_{nm} is the dipole force tensor for the loop in the cubic system. It is evaluated from the area vector and Burgers vectors b, of the loop

$$P_{nm} = (C_{12}\text{ Tr }\omega_{nm} + C_{an}\omega_{nm})\delta_{nm} + 2C_{44}\omega_{nm}, \tag{7}$$

where $\omega_{nm} = \frac{1}{2}(S_n b_m + S_m b_n)$. The subscripts n,m designate vector components, $\text{Tr }\omega_{nm} = \Sigma_i \omega_{ii}$ are defined in the cubic coordinate system. In Eq. (7), Einstein's summation convention is not implied.

The superscripts S and A in Eq. (4) refer to symmetric and antisymmetric components with respect to the deviation in the scattering vector from the reciprocal lattice point $\Delta\mathbf{H}$. The first term [Eq. (5a)] is the direct Laue scattering from the loop, the next two terms are the symmetric and antisymmetric components of the Huang scattering amplitude [Eqs. (5b) and (5c)] and the last two terms [Eqs. (5d) and (5e)] are the scattering from the displaced atoms close to the loop which have to be evaluated numerically. The last two terms are symmetric and antisymmetric only if $|\Delta\mathbf{H}| < |\mathbf{H}^0|$. At very low ΔH values, $A_2^S(\mathbf{H})$ goes to zero and $A_3^S(\mathbf{H}) = M/C$,[5] where $2M$ is the attenuation factor associated with the distortions around the loop and C is the atomic fraction of loops. Therefore, for very low ΔH values, the diffuse scattering is influenced only by the Laue scattering, Huang scattering, and the attenuation factor.

III. NUMERICAL CALCULATIONS

Equations (5a), (5b), and (5c) can be readily evaluated for any loop orientation and any combination of $\mathbf{H}^0$ and $\Delta\mathbf{H}$. The amplitudes $A_3^S(\mathbf{H})$ and $A_3^A(\mathbf{H})$ have to be evaluated numerically. For the present purposes, three types of loops were considered, (110) $[111]$, (211) $[111]$, and (110) $[100]$. Electron microscopy studies of neutron-irradiated Mo and Nb have shown that the predominant irradiation-induced defects are dislocation loops having their Burgers vector along the [111] or [100] directions, with a large shear component.[3,4] Prismatic faulted dislocation loops are not prevalent in irradiated bcc metals, presumably because of the high stacking fault energy in these metals.[3] Unfortunately, electron microscopy studies are ambiguous as to the exact orientation of the loop plane.[3] The z axis was selected perpendicular to the plane of the

loop and the displacements are written in terms of rectangular coordinates, with

$$u_1(Z/R_0, \rho/R_0, \phi), \quad u_2(Z/R_0, \rho/R_0, \phi),$$

and

$$u_3(Z/R_0, \rho/R_0, \phi),$$

in units of the Burger's vector. They were evaluated for a cylindrical grid of points with $\Delta\rho = \Delta Z = R_0/10$, $\Delta\phi = \pi/10$. The displacements were evaluated using the formula given by Ohr,[12]

$$u_i\left(\frac{\mathbf{R}}{R_0}\right) = \frac{R_0/|Z|}{4\pi N} \int_0^{2\pi} \left[\sum_{j=1}^{N} \left(\chi_i \cdot \frac{\mathbf{R}}{R_0} \right) F_i(\chi_i) \right] d\theta \qquad (8)$$

where

$$\chi_i = [\,(\cos\theta)\,\vec{i} + (\sin\theta)\,\vec{j} + t_j\vec{k}\,]/\sqrt{1+t_j^2}$$

and

$$t_j = (b+a)2 + (b-a)\cos[\,(2j-1)\pi/2N]/2.$$

b and a are given by $-(X/R_0\cos\theta + y/R_0\sin\theta \pm 1)/(Z/R_0)$, $(b<a)$. x, y, z are the rectangular coordinates of the point $\mathbf{R} = (\rho\cos\theta, \rho\sin\theta, Z)$. Equation (8) is different from the one given in Eq. (10) of Ref. 12, in that all the coordinates are scaled by the radius of the loop R_0. The authors believe, in this sense, Eq. (10) of Ref. 12 is incorrect. The function $F_i(\chi)$ depends upon the Burgers vector of the loop and elastic constants of the matrix and is given by

$$F_i(\chi) = (b_n C'_{33jn} + b_p C'_{13jn})\chi_n g_{ni}. \qquad (9)$$

In Eq. (9), b_p is the component of the Burgers vector projected onto the loop plane which also defines the direction of the x axis, g_i is the Fourier transform of the elastic Green's function in the loop coordinate system.

Isoequidisplacement contour plots of u_1 and u_3 for a sheared dislocation loop lying in the (011) plane of Nb with Burger's vector $a/2\,[\bar{1}11]$, making an angle of 35.27° with the loop normal, are shown in Figs. 3 and 4 of Ref. 12. Here the z axis is along the [011] direction and the x axis along the [$\bar{1}00$] direction. The displacement at any given point is reduced compared to similar plots for an isotropic crystal, due to the elastic anisotropy of Nb.[12] Figure 1 shows the locus of elastic displacements of constant magnitude around a dislocation loop lying on the (211) plane of Nb with Burger's vector $a/2\,[11\bar{1}]$, which makes an angle of 61.87° with the loop normal. The z axis is along the [211] direction and the x axis along the b_p or [$12\bar{4}$] direction. Displacements are plotted in the elastic region and exhibit a $1/|R|^2$ fall off. The arrows denote the direction of the displacements in the xz or [$\bar{2}31$] plane. Elastic anisotropy introduces small components along the y direction.

Figure 2 shows the calculated diffuse scattering around the (330) reciprocal lattice point scaled according to $|A(H)|^2\,[(2\pi\Delta H)^4/R_0^2]$. The intensity is plotted along both the radial ([110], [$\bar{1}\bar{1}\,0$]) and transverse [($\bar{1}10$],[$1\bar{1}0$]) directions for 5-, 10-, and 15-Å radii [211] [$11\bar{1}$] vacancy loops in Nb. In determining the diffuse scattering intensity,
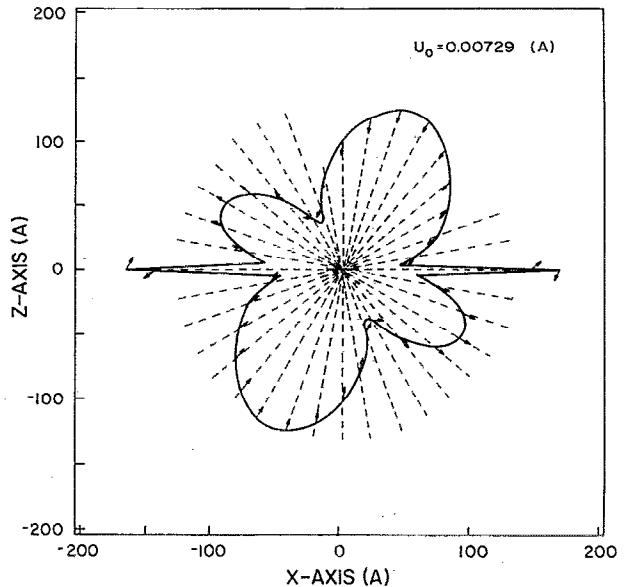

FIG. 1. Displacement of constant magnitude plotted in the ($\bar{2}31$) plane for a vacancy loop on the (211) plane with a Berger's vector $a/2\,[11\bar{1}]$. The Burger's vector projected onto the (211) is along the x axis of this figure.

the amplitudes $A_3^S(\mathbf{H})$ and $A_3^A(\mathbf{H})$, were calculated by numerically evaluating the integrals given in Eqs. (5d) and (5e) over a cylindrical volume bounded by $\rho = 5R_0$, $z = 10R_0$ around the circular loop. The contribution from atoms situated beyond $\rho = 5R_0$, $z = 10R_0$ to the amplitudes $A_3^A(\mathbf{H})$ and $A_3^S(\mathbf{H})$ is negligible. Intensities are calculated from an equally weighted average over all equivalent loop orientations, such that the cubic symmetry of the crystal is maintained. It is seen that the intensities are much larger in the transverse direction, as compared to the radial directions. In addition, for vacancy loops, there is a large directional dependence in the diffuse scattering along the radial direction about the reciprocal lattice point (i.e., the scattering along the [110] direction is much smaller than the [$\bar{1}\bar{1}\,0$] direction). The intensity plots from interstitial loops are very similar, but the intensities along the radial directions are reversed (i.e., the scattering along the [$\bar{1}\bar{1}0$] direction is much smaller than along the [110] direction). The scaled diffuse scattering show a distinct structure with maxima, that shift closer to the Bragg peak position with increasing radius of the loop. The shift approximately scales as $1/R_0$. Note that the results are very similar to the ones obtained by Larson and Young[5] in their diffuse scattering simulations from prismatic dislocation loops in fcc metals. They are explained in terms of Bragg scattering from almost constant strain regions within one radius of the loop.[5,14] A measurement of diffuse scattering around the (330) reciprocal lattice point along both the radial and transverse direction allows one to determine the type (vacancy or interstitial), concentration, and size distribution of loops. Figure 3 is a scaled ($\times[2\pi\Delta H]^4$) diffuse scattering plot illustrating the influence of loop orientation and the direction of the Burger's
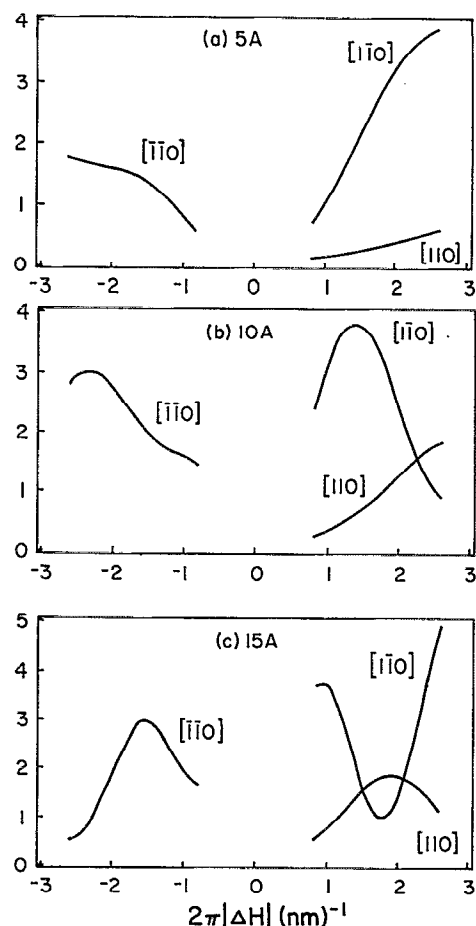
FIG. 2. Scaled theoretical diffuse scattering curves around the (330) along three designated directions. The loop plane is (211) and the Burger's vector is $a/2$ [11$\bar{1}$]. 5-, 10-, and 15-Å loops are illustrated. Multiply Y axis by 1.2×10^4 to obtain electron units per atoms/nm^4.
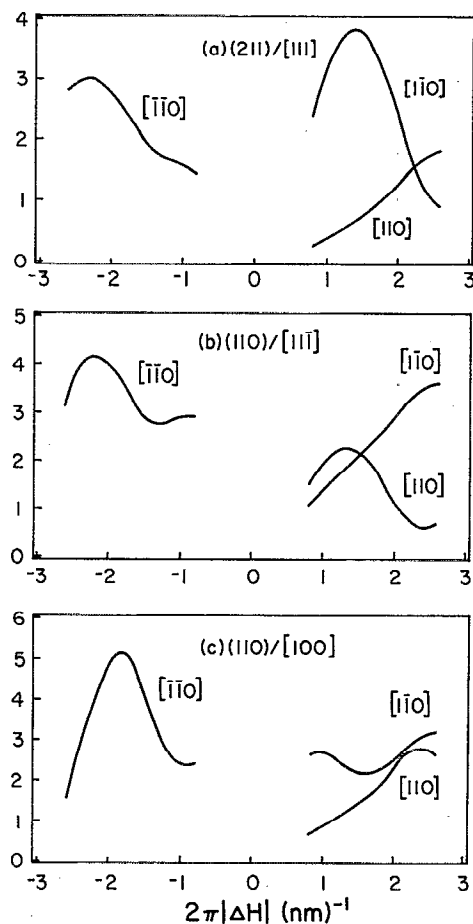

FIG. 3. Scaled theoretical diffuse scattering curves around the (330) along three designated directions. The loop plane and Burger's vector are as indicated in (a), (b), and (c). 10-Å radius vacancy loops are used for all three. Multiply Y axis by 1.2×10^4 to obtain eua/nm^4.

vector for three common arrangements. Each configuration has a unique plot. We find that (211)[11$\bar{1}$]-type loops are the predominant defects.

IV. EXPERIMENTAL DETAILS

Two single-crystal films having a (111) orientation and a thickness of 2500 Å were deposited onto (001) sapphire substrates at the Naval Research Laboratory using a vacuum of better than 10^{-10} Torr. For the x-ray diffuse scattering measurements, one of the films was used as an unimplanted standard and the other was implanted with N to an average concentration of 0.5 at. % at LNT using a four-step implantation process. The implantation sequence is shown in Table I beginning with the highest energy followed by successively lower energies. The Gaussian-like distributions become sharper at the lower energies, and are designed to superimpose with roughly a constant composition of N. The uniformity of this distribution has been examined in Ref. 7. The maximum damage energy in the implanted film produced 6 dpa.

Diffuse scattering measurements were made at the NSLS with synchrotron radiation with a wavelength of

0.8835 Å. Data were collected near the (330) peak along the radial [110], [$\bar{1}\bar{1}$0] directions and [1$\bar{1}$0][$\bar{1}$10] transverse directions. The transverse directions [2$\bar{1}\bar{1}$], [$\bar{2}$11], and [1$\bar{1}$0] directions were used to obtain data about the (222). Approximately 200 000 counts were required at each point to obtain statistically reliable results. Background from temperature diffuse and Compton scattering were removed by taking a difference between implanted and unimplanted samples giving an average of 10 000 counts per point. An absolute intensity scale was obtained using the integrated

TABLE I. Range, standard deviation (straggling), and fluences of the four implantations used to implant a Nb single-crystal film to an average level of 0.5 at. % N.

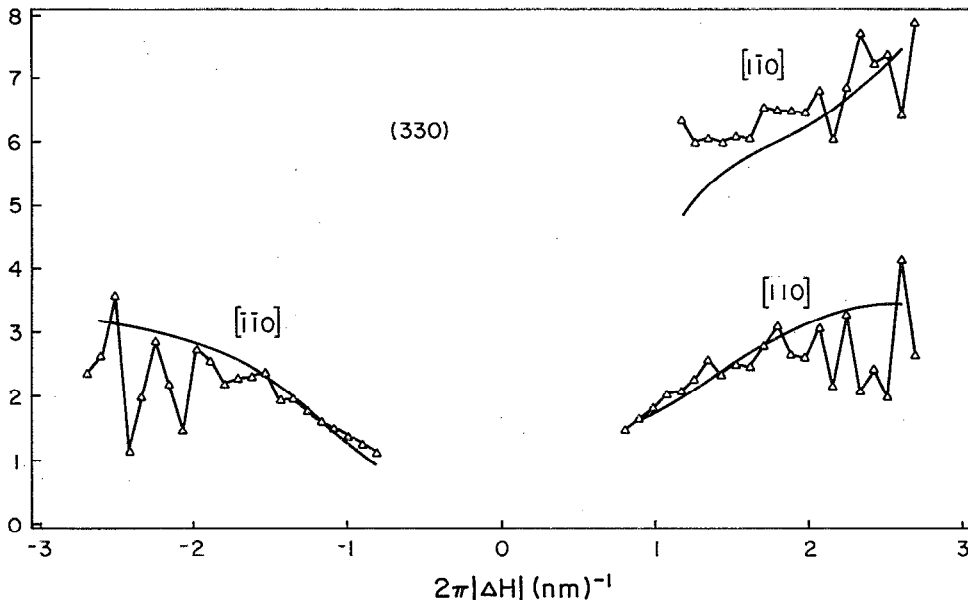| Energy (kV)	Range (Å)	Standard deviation (Å)	Fluence atoms/Å^2
190	2094	729	0.49
89	1076	463	0.20
43	559	275	0.12
17.5	259	141	0.055

FIG. 4. Scaled experimental diffuse scattering from loops and theoretical fits about (330) along three designated directions. Parameters may be found in Table I. Multiply Y axis by 1.2×10^4 to obtain eua/nm^4.

intensities of (111), (200), and (220) powder peaks from Ni.[15,16] This procedure was accurate to with $\pm 10\%$.

The measured diffuse scattering data (Fig. 4) was analyzed using Eq. (8) after multiplying by $(2\pi\Delta H)^4$. Three discrete sizes of interstitial and vacancy loops, i.e., 5, 10, and 15 Å, were used in the fitting procedure.[7] In addition, attenuation factor measurements were made on the 0.5- at. % N implant film. These data were analyzed using Eq. (5d), in the limit of $\Delta H \rightarrow 0$. In the analysis of both the diffuse scattering and attenuation factor measurements, the contribution of single N interstitials located in octahedral sites was subtracted from the experimental data. This contribution was calculated using the lattice Green's function Kanzaki force method and the force model developed for N in Nb (Ref. 2).

V. RESULTS AND DISCUSSIONS

Figure 4 shows experimentally measured diffuse scattering intensity from the implanted Nb film multiplied by $(2\pi\Delta H)^4$ for the (330) reflection along the radial ([110], [$\bar{1}\bar{1}$0]), and transverse ([1$\bar{1}$0]) directions. Figure 5 shows a similar plot for the diffuse scattering intensity calculated for single N interstitials at a concentration of 0.5 at. %. A comparison of the two plots shows that the experimental data is larger by an order of magnitude than the expected contribution from single N interstitials located in octahedral sites. In addition, the calculated data from N interstitials show a large asymmetry along the radial direction ([110], [$\bar{1}\bar{1}$0]) around the (330) reciprocal lattice point. The experimental data does not show such a pronounced asymmetry. Diffuse scattering from N clusters, assuming linear superposition of displacement fields from individual N atoms within a cluster, would also show an asymmetry that is not in accord with experimental data. Therefore, we believe that the main source of diffuse scattering from the 0.5% N-implanted Nb film shown in Fig. 4 is due to damage-related defect loops. The fact that there are almost equal amounts of diffuse scattering along both

the [110] and [$\bar{1}\bar{1}$0] directions around the (330) reflection indicates that the total number of vacancies in vacancy loops is nearly the same as the number of interstitials in interstitial loops.[5]

Electron microscopy studies of neutron-irradiated bcc metals at low temperatures and low damage energies[3,4] indicate that the predominant defect clusters formed during the irradiation process are interstitial and vacancy loops with $\frac{1}{2}$ [111]- and [100]-type Burgers vectors. Voids are expected to nucleate only after high-temperature irradiations or high-temperature anneals. Therefore, the experimental diffuse scattering data of Fig. 4, after subtraction of the 0.5- at. % N contributions of Fig. 5, was analyzed in terms of vacancy and interstitial loops. However, the data could only be fitted with loops of type (211)[11$\bar{1}$] and sizes ranging from 5-15 Å. The size range was picked from the form of the experimental diffuse scattering plot of Fig. 4 at low and high ΔH values by comparing it with the theoret-
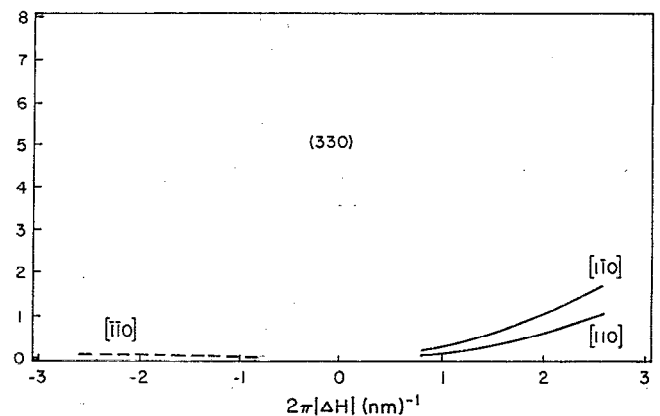

FIG. 5. Scaled theoretical diffuse scattering about (330) along three designated directions for the displacements from 0.5-at. % N in Nb. Multiply Y axis by 1.05×10^4 to obtain eua/nm^4.

TABLE II. Concentrations of vacancy and interstitial loops of different radii, per cm^3 and the total amount of point defects in loops, in a (111) single-crystal Nb film implanted with N to an average concentration of 0.5 at 0%.

Radius (Å)	$c_{\text{int.loops}}/\text{cm}^3$ $\times 10^{-18}$	$c_{\text{vacloops}}/\text{cm}^3$ $\times 10^{-19}$	N_{pd}(at. %)
5	...	1.09	0.115
10	1.64	...	0.069
15	0.221	...	0.021

ically simulated profiles for different size loops (Fig. 2). The ratio of the magnitude of experimental diffuse scattering along the transverse to the radial directions is ~3 (see Fig. 4), indicating that $(211)[11\bar{1}]$ loops are the predominant defect clusters and $(011)[111]$ and $(011)[001]$ loops are not prevalent in the implanted sample (see Fig. 3). A linear least-squares fit of the experimental data with respect to the concentration of $(211)[11\bar{1}]$ vacancy and interstitial loops of sizes 5, 10, and 15 Å is shown in Fig. 4. The concentrations of vacancy and interstitial loops per unit volume, of radii 5, 10, and 15 Å, obtained from the linear least-squares fit is given in Table II. Table II also gives the concentration of single vacancies and interstitials retained in the implanted sample which are located in loops.

Additional data were collected to confirm the results of Table II. Figure 6 shows the experimental diffuse intensity around the (222) reflection averaged over the two symmetrical transverse directions, $[11\bar{2}]$, and $[\bar{1}\bar{1}2]$. The overall agreement between theory and experiment is shown for $(211)[11\bar{1}]$ and $(110)[1\bar{1}1]$ loops. Again, one finds the best agreement with $(211)[11\bar{1}]$ loops.

Vacancy loops are predominantly 5 Å in radius, whereas the interstitial loops are distributed over the range 10–15 Å. Interstitial loops are expected to be larger in size as compared to vacancy loops, because of the higher mobility of self-interstitials as compared to vacancies. This size difference has been found after several types of irradiations into Cu.[5,17] The ratio of the total number of vacancies to total number of interstitials, retained in the implanted sample, in loops, would seem to indicate that self-interstitials are lost at sinks such as dislocations or interfaces, which are present in the unimplanted sample. However, the total concentration of single vacancies in the irradiated film, in loops, is 0.11 at. % and for single interstitials, 0.095 at. %. This small difference is within the error of our analysis.

Attenuation factor data,[7] obtained from the reduction of the integrated intensities, is in agreement with the proposed loop model and with N located in octahedral positions. This agreement, using the data of the preceding paragraph as well as the N level already cited for the 0.5- at. % sample, represents additional confirmation of the simple model for N implanted into Nb. Our results for the implanted Nb films are similar to the ones obtained in Ref. 5, for neutron and ion irradiations of single crystal Cu at 4 K and a lower damage energy. In both cases, loops of small size are found with nearly the same number of interstitials and vacancies. The major difference between our results and the previous results is that the average radius of the loops is approximately $\frac{1}{2}$ of what was found in irradiated Cu. One difference may be associated with the high stacking fault energy in bcc metals which results in the formation of unfaulted loops with a large shear component.[3,4] These x-ray measurements do not unambiguously establish that the vacancy-type clusters are dislocation loops,[5] particularly if one considers the small size of the loops. However, the presence of similar scattered intensity at negative ΔH values in Fig. 4 does establish that the total collapsed volume is essentially equal to the interstitial loop volume.

VI. CONCLUSIONS

The following conclusions have been reached.

(i) X-ray diffuse scattering from a 2500 Å, (111) single-crystal Nb film, implanted to 0.5 at. % N at LNT, arises predominantly from damage-related clusters formed during the irradiation process.

(ii) The damage-related clusters are identified to be $(211)[11\bar{1}]$-type vacancy and interstitial loops. Vacancy loops have predominantly a 5-Å radius. The interstitial loops are of larger radii, i.e., 10–15 Å. The data were fitted with 75% of the interstitials retained as 10-Å loops and 25% as 15-Å loops. The total amount of vacancies or interstitials retained in the film in loops were found to be ~0.10 at. %.
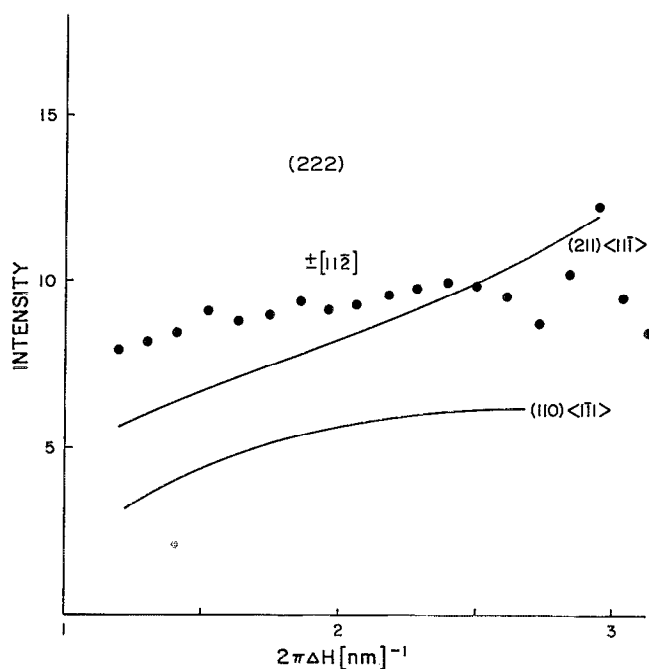

FIG. 6. Experimental diffuse scattering points along designated directions and theoretical curves about the (222) from $(211)[11\bar{1}]$, $(110)[1\bar{1}1]$ loops. Multiply Y axis by 1.02×10^4 to obtain eua/nm^4.

ACKNOWLEDGMENTS

[1] H. Dosch and J. Peisl, Phys. Rev. B **32**, 623 (1985).
[2] Satish I. Rao, E. J. Savino, and C. R. Houska, Mater. Res. Soc. Symp. Proc. **82**, 187 (1987).
[3] M. Wilkens, in *Diffraction and Imaging Techniques in Materials Science*, 2nd ed., edited by S. Amelinckx, R. Gevers, and J. Van Landuyt (1979), Vol. 2, p. 185.
[4] B. L. Eyre, M. H. Loretto, and R. E. Smallman, in *Vacancies* 76, edited by R. E. Smallman and J. E. Harris (1977), p. 630.
[5] B. C. Larson and F. W. Young, Jr., Phys. Status Solidi A **104**, 273 (1987).
[6] B. C. Larson and W. Schmatz, Phys. Status Solidi B **99**, 267 (1980).
[7] S. I. Rao, B. He, C. R. Houska, and K. Grabowski, J. Appl. Phys. Companion paper.
[8] S. I. Rao, C. R. Houska, K. Grabowski, J. Claaussen, G. Ice, and H. Habenschuss, Mater. Res. Soc. Symp. Proc. **138**, 87 (1989).
[9] P. H. Diederichs, J. Phys. F **3**, 471 (1973).
[10] P. Erhart, H. Trinkaus, and B. C. Larson, Phys. Rev. B **25**, 325 (1982).
[11] M. A. Krivoglaz, *Theory of X-ray and Thermal Neutron Scattering by Real Crystals* (Plenum, New York, 1969).
[12] S. M. Ohr, Phys. Status Solidi B **64**, 317 (1974).
[13] D. Frederick and T. S. Chang, *Continuum Mechanics* (Scientific, Boston, 1972).
[14] H. Trinkaus, Z. Angew, Phys. **31**, 229 (1971).
[15] P. Suorti, J. B. Hastings, and D. E. Cox, Acta Cryst A **41**, 413 (1985).
[16] P. Suorti, J. B. Hastings, and D. E. Cox, Acta Cryst. A **41**, 417 (1985).
[17] H. Matea, B. C. Larson, T. P. Sjoreen, D. K. Thomas, O. S. Oen, and J. D. Lewis, Mater. Res. Soc. Symp. Proc. **138**, 81 (1989).